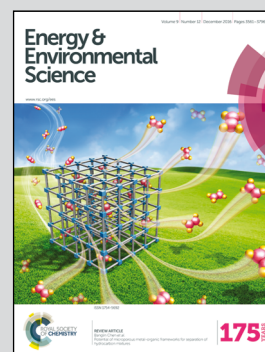


Showcasing research from a collaborative team of scientists at the National Institute of Standards and Technology and the National Renewable Energy Laboratory, Colorado, USA.

Methylammonium lead iodide grain boundaries exhibit depth-dependent electrical properties

Inorganic–organic perovskite active layers have shown great promise as photoactive layers for solar energy conversion. The electrical properties of grain boundaries (GB) in these materials, as well as the impact of these properties on the power-conversion efficiency of completed devices, has been hotly debated. We show, for high efficiency large-grain methylammonium lead iodide thin films, that a depth-dependent resistance ($R_{GB}(z)$) is present, as well as considerable GB-to-GB heterogeneity in the electrical properties.

As featured in:



See Frank W. DelRio et al., *Energy Environ. Sci.*, 2016, 9, 3642.

CrossMark
click for updates

Methylammonium lead iodide grain boundaries exhibit depth-dependent electrical properties†

Cite this: *Energy Environ. Sci.*,
2016, 9, 3642Received 1st July 2016,
Accepted 23rd September 2016Gordon A. MacDonald,^a Mengjin Yang,^b Samuel Berweger,^c Jason P. Killgore,^a
Pavel Kabos,^c Joseph J. Berry,^d Kai Zhu^b and Frank W. DelRio^{*a}

DOI: 10.1039/c6ee01889k

www.rsc.org/ees

In this communication, the nanoscale through-film and lateral photo-response and conductivity of large-grained methylammonium lead iodide (MAPbI₃) thin films are studied. In perovskite solar cells (PSC), these films result in efficiencies >17%. The grain boundaries (GBs) show high resistance at the top surface of the film, and act as an impediment to photocurrent collection. However, lower resistance pathways between grains exist below the top surface of the film, indicating that there exists a depth-dependent resistance of GBs ($R_{GB}(z)$). Furthermore, lateral conductivity measurements indicate that $R_{GB}(z)$ exhibits GB-to-GB heterogeneity. These results indicate that increased photocurrent collection along GBs is not a prerequisite for high-efficiency PSCs. Rather, better control of depth-dependent GB electrical properties, and an improvement in the homogeneity of the GB-to-GB electrical properties, must be managed to enable further improvements in PSC efficiency. Finally, these results refute the implicit assumption seen in the literature that the electrical properties of GBs, as measured at the top surface of the perovskite film, necessarily reflect the electrical properties of GBs within the thickness of the film.

Organolead trihalide perovskites, such as MAPbI₃, have seen rapid development for solar applications since their first demonstration in sensitized solar cells in 2009.^{1–8} The present maximum certified efficiency for perovskite solar cells (PSCs) now exceeds 22%.⁹ Many questions remain about how these polycrystalline thin films, which are typically solution cast, operate in photovoltaic applications. In particular, it is still unclear what role surface and grain boundary (GB) charge traps

Broader context

Organic–inorganic perovskites have attracted significant attention from the scientific community due to their great potential as constituent materials in low-cost, scalable, and highly efficient photovoltaic devices. However, many questions remain about how these polycrystalline thin films operate in photovoltaic applications, and in particular, what role the electrical properties of grain boundaries (GBs) play in determining the overall properties of films and performance of devices. As a result, there has been a research focus in recent years that attempts to construct a physical model for the electrical and photophysical processes that occur at GBs. In this communication, we show that large-grained methylammonium lead iodide GBs exhibit GB-to-GB heterogeneity and depth-dependence in electrical properties. At the top surface of the film, the GBs exhibit high resistance and act as impediments to photocurrent collection. Below the surface, there exist less resistive pathways that can typically be overcome *via* electrical fields and low levels of photoexcitation. However, there is considerable variability in the local lateral resistance, resulting in collections of grains with lower lateral conductivity as well as some grains that are electrically isolated from the surrounding film. Altogether, this information can be used to target processing conditions designed to specifically address the structure of GBs in order to control the properties and maximize the performance of these promising materials.

play in the overall properties of the films and what the best approaches are for further increasing the efficiency and stability of these promising materials. The answer to the first question may provide insight into the second question, as GBs are known to play a critical role in the charge carrier dynamics and photophysics of thin-film photovoltaic active layers, such as CdTe, CIGS, poly-Si, *etc.*^{10–12} As a result, there has been considerable research in recent years that attempts to construct a physical model for the electrical and photophysical processes that occur at the GBs of MAPbI₃ and related perovskite active layers.^{13–17} However, there continues to be disagreement in the community about the role that GBs play in the electrical and photophysical properties of device-relevant films of these materials. Some studies have suggested that GBs act as non-radiative recombination centers.^{13,18} In another study, it was suggested that GBs are passivated *via* conversion to lead iodide,¹⁵ which

^a Applied Chemicals and Materials Division, Material Measurement Laboratory, National Institute of Standards and Technology, Boulder, CO 80305, USA. E-mail: frank.delrio@nist.gov

^b Chemistry and Nanoscience Center, National Renewable Energy Laboratory, Golden, CO 80401, USA

^c Applied Physics Division, Physical Measurement Laboratory, National Institute of Standards and Technology, Boulder, CO 80305, USA

^d National Center for Photovoltaics, National Renewable Energy Laboratory, Golden, CO 80401, USA

† Electronic supplementary information (ESI) available. See DOI: 10.1039/c6ee01889k

minimizes non-radiative recombination. Still other researchers have come to the conclusion that GBs lead to higher photocurrent collection due to more efficient charge carrier separation and transport,¹⁴ or contribute to current density (J)-voltage (V) hysteresis due to ion-migration.¹⁷

In this communication, device-relevant MAPbI₃ thin films are examined with conductive-probe atomic force microscopy (C-AFM) and photoconductive atomic force microscopy (pc-AFM) to investigate the electrical properties and electrical property heterogeneity at GBs. We examine the electrical properties of GBs, and their associated effects on in-plane and through-thickness electrical properties as well as local photocurrent response. For a large-grained MAPbI₃ thin-film with >17% efficiency in PSC devices, it is shown that GBs impede photocurrent (pc) collection and that the GBs are highly electrically resistive at the top surface of the film. We also demonstrate that, beneath the top surface of the film there exist less resistive, lateral conduction pathways across most GBs. These pathways may contain significant physical and/or energetic barriers at GBs. However, these lateral barriers can be overcome *via* electrical fields and low levels of photoexcitation, while the high electrical resistance at GBs in through-film measurements remains even under applied fields and photoexcitation. Furthermore, while most GBs must exhibit sufficient lateral conductivity to allow for measureable lateral currents under our experimental conditions, the high electrical resistance of certain GBs results in groups of grains that show a reduced electrical response and certain grains that are near-completely electrically isolated from the surrounding film.

The high electrical resistance at the top of GBs, coupled with the variation in the effective lateral resistance under applied electric fields and photoexcitation, strongly implies that the electrical properties of GBs vary not only from GB-to-GB, but also as a function of depth (z) from the top surface of the film. That is to say that the resistance of GBs (R_{GB}) is a function of z . To date, all studies have examined the properties at the top surface of organic-inorganic films (*e.g.*, surface workfunction and conductivity) and have assumed that the GB properties measured at the top-surface of the film are representative of the properties of the GBs within the thickness of the film. While this may be the case in some circumstances, there is no clear physical or chemical reason to assume this to be true *a priori*. Unlike previous studies in the literature, this work tests this assumption and finds a significant difference in the electrical properties of GBs at the top surface of these films as compared to the subsurface electrical properties. These results will help guide researchers towards targeted approaches that account for the variation in the GB properties as a function of depth into the film.

MAPbI₃ active layers and devices were prepared *via* the solution process recently reported by Yang *et al.*¹⁹ for PSC devices. The MAPbI₃ active layer was *ca.* 350 nm thick for all experiments and devices. The architecture consisted of fluorine-doped tin oxide (FTO)/compact TiO₂/MAPbI₃/2,2',7,7'-tetrakis (*N,N*-dip-methoxy-phenylamine)-9,9'-spirobifluorene (Spiro-MeOTAD) hole transport layer, and an Ag top contact. A schematic of the completed PSC device is shown in Fig. 1a. Further details on the PSC device

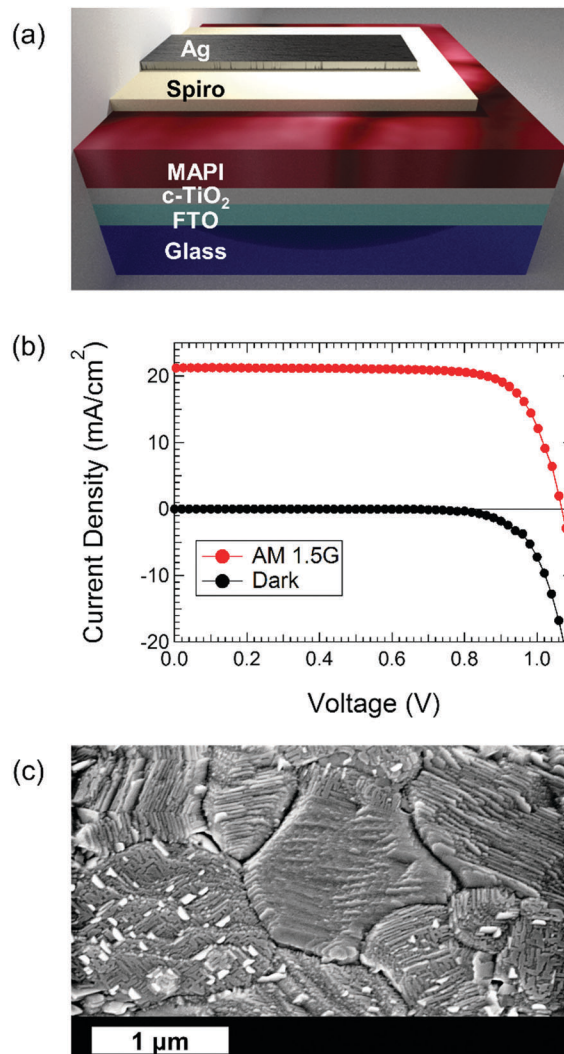


Fig. 1 (a) Schematic of the PSC device stack. (b) The dark and AM 1.5G (100 mW cm⁻²) illuminated J - V response of a typical FTO/TiO₂/MAPbI₃/Spiro-MEOTAD/Ag device. (c) SEM image of the MAPbI₃ layer. The MAPbI₃ grains are typically ≈ 1 μ m in diameter, and show distinct grain boundaries.

fabrication can be found in the ESI.† This process resulted in MAPbI₃-based PSC devices with short-circuit current density (J_{sc}) and open-circuit voltage (V_{oc}) of 21.2 mA cm⁻² and 1.07 V, and a power conversion efficiency (PCE) of 17.3% under reverse scan (100 mV s⁻¹), as shown in Fig. 1b. These devices did show some hysteretic behavior, but maintained a stabilized PCE of >17% as shown in Fig. S1a and b in the ESI.† The efficiency observed for devices produced by this method is among the state-of-the-art efficiencies to-date for planar standard PSC devices.^{8,19,20} Scanning electron microscopy (SEM) images of the MAPbI₃ thin films (Fig. 1c) indicate grains that are typically *ca.* 1 μ m in diameter and show distinct grain boundaries. Additionally, the clear striations on the grain surfaces suggest that these films are highly crystalline. Previous studies have shown that this process leads to high quality, highly uniform, textured, and pinhole free MAPbI₃ layers, which results in PSC devices with high stabilized PCEs of >15% for devices with active areas as large as 1.2 cm².¹⁹

The height and photocurrent response of a MAPbI₃ active layer on a FTO/TiO₂ stack are shown in Fig. 2a and b, respectively. Measurements were taken under a dry N₂ environment. A 523 nm wavelength LED was used for illumination and was focused onto the sample with a spot diameter of *ca.* 440 μm. The intensity of illumination was *ca.* 100 mW cm⁻² (further details on the pc-AFM setup are in the ESI†). The AFM probe used in this study was coated with a conductive iridium layer and had a nominal tip radius of 28 nm. Due to the high workfunction of Ir (*ca.* 5.3 eV) and the hole blocking characteristics of TiO₂, the current collected at the probe is due to the collection of photogenerated holes. The average value for the photocurrent in Fig. 2b is *ca.* 175 pA. Assuming that the photocurrent response for FTO/TiO₂/MAPbI₃/Ir is less than or equal to that for the FTO/TiO₂/MAPbI₃/Spiro-MEOTAD/Ag device, we can calculate a lower limit for the effective charge collection area (A_{eff}) from $A_{\text{eff}} = I_{\text{pc}}/(J_{\text{SC}} \times F)$, where A_{eff} assumes zero lateral diffusion from outside the electrode area, I_{pc} is the average photocurrent from pc-AFM (Fig. 2b), J_{SC} is the short-circuit current density from the completed device (Fig. 1b), and F is a ratio of the number of charge-generating photons from the LED light source divided by the number of charge generating photons from the solar spectrum (in this case $F \approx 2$). For $I_{\text{pc}} = 175$ pA and $J_{\text{SC}} = 21.2$ mA cm⁻², A_{eff} is *ca.* 0.41 μm². This leads to an effective collection diameter of *ca.* 700 nm. The AFM tip-sample contact diameter is estimated to be <10 nm based on a Hertzian mechanics model of the tip-sample contact.²¹ Therefore, A_{eff} is approximately three orders of magnitude greater than the tip-sample contact area (<300 nm²). We did not observe any

significant variation in the photocurrent of large grains (>700 nm diameter) as compared to smaller grains (<700 nm diameter), nor did we observe a decrease in the photocurrent hundreds of nanometers away from GBs. From this result, we conclude that the high mobility and charge carrier lifetimes in the MAPbI₃ allow for photogenerated holes to travel several hundred nanometers from the location of the initial photoexcitation prior to collection at the conductive probe, and that many photogenerated holes laterally cross one or more GBs prior to collection. We note that the electrical field associated with the photovoltage in pc-AFM is likely to have a significant lateral component, based on the point-plane geometry of the electrodes in this experiment. Thus, the driving force for lateral motion of charges across GBs is greater under these circumstances than in the case of either completed planar devices or for samples with zero or one contact, as used in spatially-resolved photoluminescence studies.

Additionally, it is important to note the variations in the photocurrent response related to both GBs as well as striations on the grains themselves. The results indicate that GBs impede the collection of photocurrent, at least locally near the top surface of the film. It is well established that the measured current in conductive-probe AFM measurements increases with increasing tip-sample contact area.²² The contact area between the probe and the sample can increase dramatically, due to both the local curvature of the sample resulting in contact between the sample and the side of the probe tip, as well as increased contact forces due to the lag-time of the z-piezo feedback response while tracking up a feature. Therefore, if the electrical properties of the sample were perfectly uniform, then one would expect to measure a higher current at GBs due to the increased sample slope in these regions. Interestingly, we observe zero photocurrent at GBs, and thus our measurement cannot be attributed to topography-related artifacts.

Previous pc-AFM studies have also established a relationship between GBs and measured photocurrent on active layers.^{14,23} The results presented here are in direct contradiction to the results of Yun *et al.*,¹⁴ who reported an increased photocurrent collection at GBs. At this time, it is unclear if the difference between these results is due to differences in the processing conditions of these films, or if the higher photocurrent observed by Yun *et al.* at GBs is due to the higher contact area between the tip and the sample in the concave grain boundaries. In contrast, Li *et al.* demonstrated a reduction in the photocurrent response at GBs without an externally applied bias similar to the results presented in this work.²³ Unlike Li *et al.*, we did not observe an increase in current at GBs when the sample was illuminated under a small positive bias.

Fig. 2c shows typical current (I)- V sweeps taken near the center of an individual grain. In these experiments, V was swept from 0 V to +1 V, +1 V to -1 V, and -1 V to +1 V, sequentially, while under illumination. The I - V response was strongly hysteretic, and exhibited a greater hysteresis than that observed for the completed MAPbI₃-based PSC devices (Fig. S1a, ESI†). However, the current at 0 V in the 0 V to +1 V sweep is in good agreement with the I_{pc} results from Fig. 2b, which indicates that the photocurrent measured as the probe is scanned over an area does not

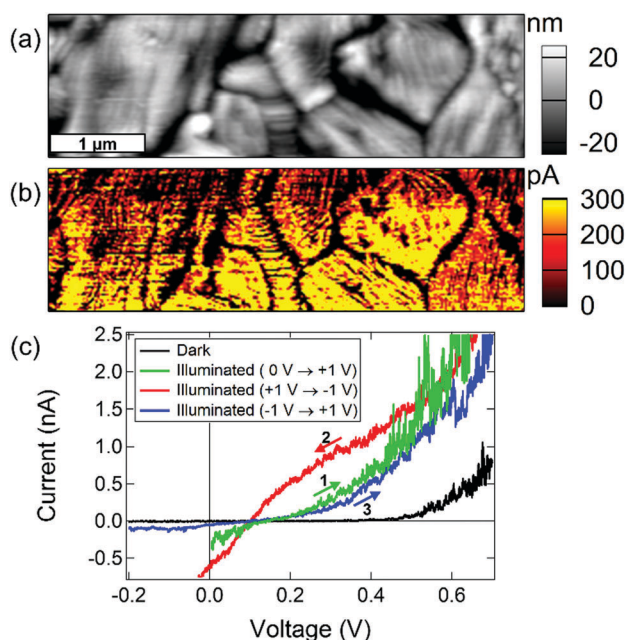


Fig. 2 pc-AFM (a) height and (b) photocurrent data with no applied voltage and 100 mW cm⁻² photoexcitation with a 523 nm light-emitting diode on a FTO/TiO₂/MAPbI₃ sample. Photocurrent is impeded at GBs. (c) Typical I - V response taken near a grain center with ≈ 170 nN applied force.

result from significant non-Faradaic current, *e.g.* ion migration related to the moving electrical field as the probe is scanned across the surface. Moreover, it is important to note that the V_{OC} results from Fig. 2c are significantly lower than those for the completed devices in Fig. 1a. This reduced V_{OC} is likely due, at least in part, to the absence of a hole transport layer (HTL). HTLs can drastically reduce surface trap states,¹⁶ and prevent the direct contact of the metal tip with the MAPbI₃ thin film, which may lead to metal-assisted quenching of photogenerated charges, particularly at low internal fields. The striations observed on the grains limit the collection of photocurrent. This may be due to preferential formation of PbI₂,^{15,20} or perovskite hydration products,²⁴ at crystallographic steps. We note that the pc-AFM measurements were performed under a dry N₂ environment, and the results did not show evidence of significant changes in the morphology or photoconductivity response over the course of several hours.

C-AFM measurements were performed to determine if the striations were limited to a surface effect. As shown in Fig. S2 in the ESI,[†] the striations can be removed by scanning at a sufficient force and/or through repeated scanning in the same location. The GBs remain resistive under both reverse bias (*i.e.* h⁺ collection at AFM probe) (Fig. 3) and forward bias (*i.e.* h⁺ injection at AFM probe, not shown). This indicates that the absence of a measurable photocurrent at the GBs in this system is due to a larger electrical resistance for hole transport in the vicinity of GBs. The frequency distribution plot of the current response, Fig. 3c, indicates a bimodal electrical response with one maximum near zero and one near 170 pA. Further studies are needed in order to determine the cause of the high resistance at GBs. The high resistance may be due to degradation of the material at the GBs to PbI₂,^{15,20} by the preferential formation of perovskite hydrates at GBs,^{25,26} and/or the development of a high concentration of trap states at the top surface of GBs that reduces the local hole charge carrier density.

Previous reports have observed variation in the local surface potential, proportional to the local workfunction, of GBs *vs.* grains with Kelvin-probe force microscopy (KPFM).^{14,15,19} Based on this observation, it is important to consider whether the current response measured in Fig. 2 and 3 is dominated by the local conductivity of the sample or if a nano-Schottky diode forms between the tip and the sample. The observed variations in the local surface potential between grains and GBs in these studies was estimated to be *ca.* 30 meV to 40 meV. This is less than a factor of 1.5 greater than the thermal voltage at room temperature, *ca.* 26 meV. The current response of nano-Schottky diodes is expected to follow the equations for thermionic emission and tunnelling currents, where the dominant mechanism depends on factors such as the diode area and the applied electric field.²⁷ If a Schottky barrier were to form at the probe-sample contact, such small variations in the local surface potential would not lead to orders of magnitude change in current across the junction. For a detailed discussion which demonstrates that the local variation in the surface potential is insufficient to lead to the current variations that we observe in Fig. 2 and 3, the reader is referred to the ESI.[†]

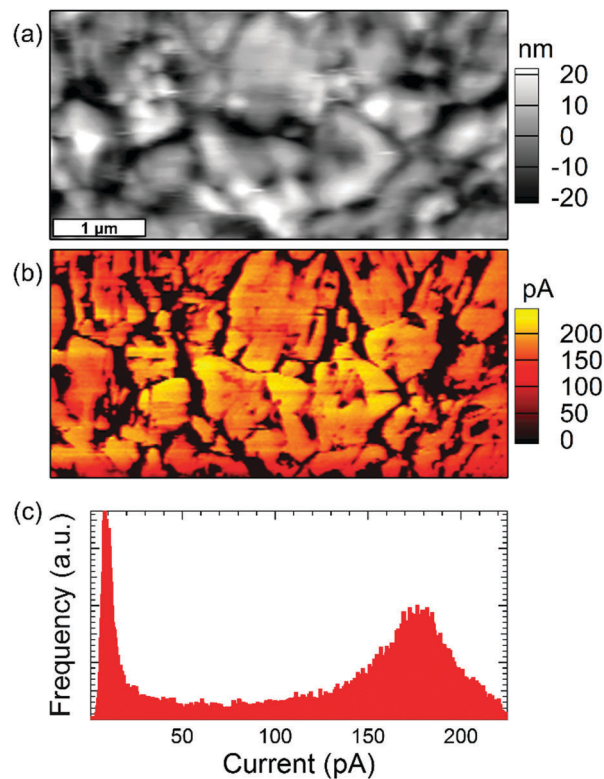


Fig. 3 C-AFM (a) height data, (b) current data, and (c) a frequency distribution plot of the current data for a FTO/TiO₂/MAPbI₃ sample. C-AFM data collected under dark conditions and 2.5 V reverse bias with ≈ 170 nN applied force.

Since neither topographical artifacts nor variations in the local surface potential can explain our results, we conclude that the differences in measured current at GBs *vs.* grains are dominated by differences in the local conductivity.

The results presented above indicate that GBs are resistive, at least at the top surface for MAPbI₃ layers fabricated in this manner, but provide no insight into $R_{GB}(z)$, *i.e.* are grains electrically isolated from other grains by GBs or are there lower resistance pathways below the top surface of the film? Indeed, most if not all, of the discussions in the literature to date that have discussed the electrical properties of organic-inorganic perovskite GBs have been based on surface measurements and the implicit assumption that the properties observed at the top surface of the film represent the electrical properties of GBs within the thickness of the film. Given the drastic difference in trap state density observed by Shao *et al.* between the top and bottom surface of MAPbI₃ thin films,¹⁶ and the depth dependence observed in cathodoluminescence microscopy reported by Bischak *et al.*,¹⁸ it is reasonable to suspect that GBs may also show a depth-dependent variation in properties, such as chemical composition.

The formation of insulating PbI₂ at GBs specifically has been proposed to reduce recombination at GBs for MAPbI₃,¹⁵ but would not contribute to the photocurrent, consistent with Fig. 2. Thus, it is expected that there will be an ideal thickness for this inter-grain insulating region. If a depth-dependence, or

GB-to-GB variation, in the electrical properties of GBs in optimized films were to occur, this would indicate that the buffer layer is likely to be too thin in some areas to effectively act as a buffer layer and/or be too thick in some regions thus unnecessarily reducing the volume of photoactive material. Indeed this is in agreement with the results of Ke *et al.* who have recently reported that the addition of $\text{Pb}(\text{SCN})_2$ as an additive for MAPbI_3 processing leads to both an increase in grain size and an increase in the formation of PbI_2 at GBs with increasing additive concentration.²⁰ In their results, increasing the concentration of $\text{Pb}(\text{SCN})_2$ up to 5% by weight in the precursor solution led to an improvement in device performance. However, further increases in the $\text{Pb}(\text{SCN})_2$ concentration led to a reduction in the device efficiency. Electrical isolation of grains could also lead to artificially high photoluminescence responses in spatially-resolved photoluminescence measurements by preventing lateral diffusion of photogenerated charges from the location of the photoexcitation and photoluminescence collection. To gain further insight into the aforementioned points, two-probe electrical measurements were conducted to assess the heterogeneity in the lateral conductivity in these films.

Fig. 4a shows a schematic of the two-probe lateral measurements used in this study. Probe 1 was scanned with the AFM, while probe 2 was fixed to the sample, such that only the probe tip was in direct electrical contact with the MAPbI_3 layer. We note that special precautions were needed to minimize damage to the thin film during the mounting of probe 2. These precautions are detailed in the ESI.† The location of the stationary probe tip (probe 2) is indicated in the height and current data by an inverted white triangle. The applied bias between probes 1 and 2 was 3 V. The topography in this region is shown in Fig. 4b, and indicates that the average grain size and morphology of MAPbI_3 on glass are similar to those of MAPbI_3 on FTO/TiO_2 . A low level of illumination was necessary in order to measure a current response. This may be due to some minor damage of the MAPbI_3 surface during the mounting of probe 2. This likely led to a less than ideal contact between probe 2 and the MAPbI_3 surface. Regardless, the contact was sufficient to investigate the relative local conductivity of the sample.

In Fig. 4c, we observe collections of grains with similar local lateral conductivity, as well as some highly electrically isolated grains, as indicated by white ovals in Fig. 4b and c. The current

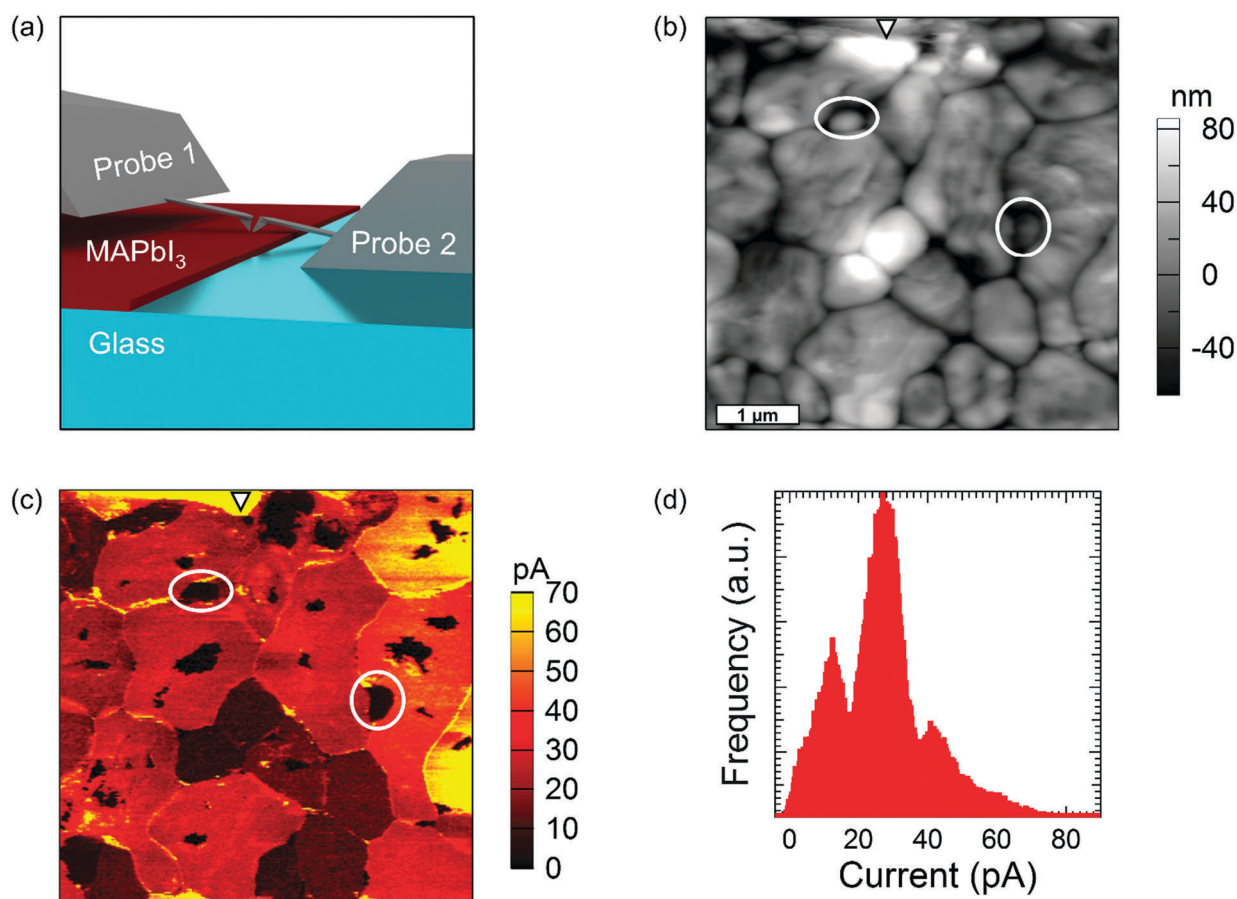


Fig. 4 (a) Schematic of the two-point lateral conductivity measurement. The sample is MAPbI_3 on glass. Probe 1 is scanned over the surface, while probe 2 is affixed to the sample, such that only the probe tip is in contact with the MAPbI_3 thin film. A bias of 3 V was applied between probes 1 and 2. The location of the stationary probe tip is shown by a white triangle in the height data (b) and current data (c). A 523 nm illumination with *ca.* 0.6 mW cm^{-2} intensity was applied while scanning. White ovals in (b) and (c) indicate the locations of grains that are highly electrically isolated from the surrounding film. (d) Frequency histogram of the current data demonstrating distinct levels of lateral conductivity.

frequency distribution plot, Fig. 4d, indicates multimodal (>3) current distributions as a result of variable lateral conductivity across GBs. This is in stark contrast to the bimodal current distribution and observed grain-to-grain homogeneity for through-film measurements in Fig. 3c, and is a strong indicator that there is a variable and depth-dependent profile to the resistance of GBs, $R_{GB}(z)$.

We note that there is a correlation between the GBs observed in the height response and a current response. In this measurement, many GBs appear more conductive than their adjacent grains. This appears to be an artifact which results from GBs acting as “lateral capacitors” when they are between the two probes. As the probe crosses a GB the lateral capacitor discharges, resulting in an increased current at the GBs that is not due to higher local conductivity. This effect is discussed in more detail in the ESI.†

In addition to the highly electrically isolated grains, there are also low current regions within certain grains in Fig. 4c. These correspond to features on the surface of the grains. These are most likely the result of the formation of PbI_2 crystals on the surface of the film during fabrication. Otherwise, the current across a grain is found to be nearly uniform. The apparent grain size observed topographically and the apparent grain size observed electrically are equivalent, which suggests that the apparent lateral grain sizes observed by AFM and SEM for this system are the true lateral grain sizes. This is in agreement with the recent findings of Reid *et al.*, who reported a strong correlation between the effective grain size extracted from gigahertz-frequency charge carrier mobility measurements and the apparent grain size observed in SEM measurements.²⁸

In Fig. 5a–c, we schematically depict the physical models of organic–inorganic trihalide GBs presented in previous studies, and in Fig. 5d, we present a depth-dependent model consistent with the results presented in this work. The models suggested in the literature include: traps at GBs which lead to increased trap-assisted recombination,^{13,18} (Fig. 5a), formation of insulating products at GBs (PbI_2 or a perovskite hydration product)

which results in a passivation layer at GBs that minimizes trap-assisted recombination,¹⁵ (Fig. 5b), and hole-transport highways at GBs which results in improved hole collection,¹⁴ (Fig. 5c). In the case of an insulating material formed at GBs, Fig. 5c, we note that the effective resistance of such a GB would be proportional to the thickness of this intergranular region.

In our system, which has been shown to result in high-efficiency $MAPbI_3$ -based PSC devices,¹⁹ we observe experimental evidence that is most consistent with the model presented in Fig. 5b, but observe no evidence to support the model presented in Fig. 5c. Moreover, the absence of I_{pc} observed in pc-AFM as well as the absence of I under far reverse bias at GBs is also consistent with the model presented in Fig. 5b. Furthermore, the lateral measurements in Fig. 4 indicated regions that are completely electrically isolated from surrounding grains, also consistent with the model in Fig. 5b. However, most of the GBs are sufficiently conductive, such that low levels of photoexcitation result in a laterally conductive pathway under an applied bias. Thus, the following points can be concluded from the results: (1) all GBs in the $MAPbI_3$ active layers under study are electrically resistive at the top surface of the film, (2) some of the GBs are resistive through the entire thickness of the $MAPbI_3$ layer (*i.e.* similar to the model in Fig. 5b) and finally (3) since less resistive pathways can be observed across GBs in lateral measurements, there must exist a depth-dependence of GBs ($R_{GB}(z)$) such that there exists a lower resistance pathway in the subsurface of the film that allows for measurable currents across most, but not all, GBs in the film.

We hypothesize that GB-to-GB variations in $R_{GB}(z)$ result in the heterogeneity in the lateral conductivity that is observed in Fig. 4. The measurements presented in this work cannot determine the profile of $R_{GB}(z)$, as both hypothetical profiles in Fig. 5d are consistent with our observed results. However, since ambient moisture has been proposed to act as a catalyst for degradation of $MAPbI_3$ to PbI_2 ,^{29,30} and diffusion of MAI into the surrounding environment is a driving factor for the degradation reaction, it is likely that the material at the top

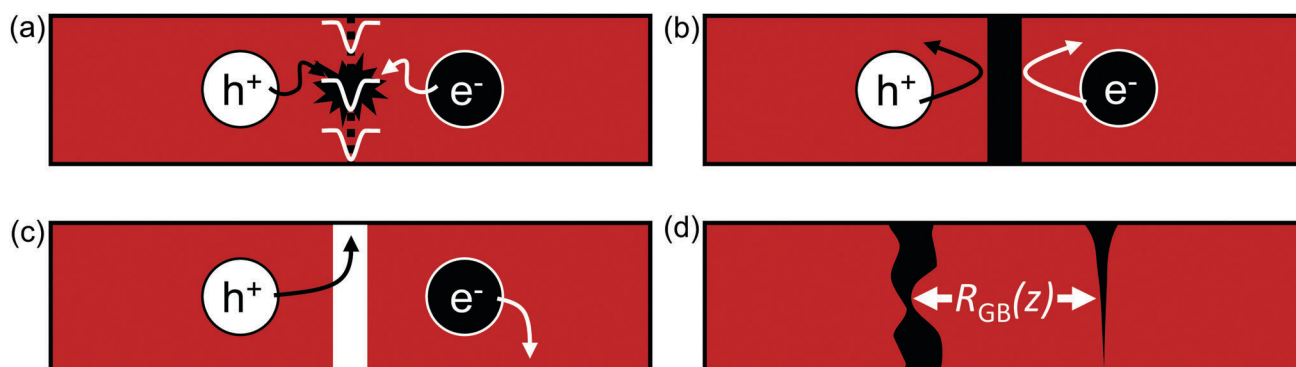


Fig. 5 Physical models for the electrical properties of GBs presented in the literature include: (a) GBs contain trap states that increase non-radiative recombination, (b) GBs are passivated *via* the formation of PbI_2 insulating “buffer-layers” between grains, and (c) GBs can act as hole-transport highways which maximize hole collection. The results of this study indicate that most GBs in this system are electrically resistive at the top surface of the film. However, lateral conduction pathways are available between most grains, below the top surface of the film, indicating that physical or electrical barriers at GBs are smaller below the top surface of GBs leading to a depth-dependence resistance ($R(z)$) as illustrated in (d). Two possible GB profiles that could lead to the observed differences in through film vs. lateral conduction are shown in (d).

surface of GBs will degrade at a faster rate than material that is below the top-surface of the film. This would be expected to lead to a reduced lateral resistance with increasing depth, as proposed in the rightmost GB presented in Fig. 5d. Furthermore, the properties of individual GBs, such as the misalignment angle between adjacent grains, are expected to impact the diffusion rate of moisture into the thickness of the film and the diffusion rate of MAI out of the film. These effects may explain why we observe heterogeneity in the lateral resistance. In all, the results indicate that GBs exhibit depth-dependent electrical properties and that the electrical properties of GBs are heterogeneous. Improved control of GB properties is expected to be important for further improvement of these materials.

Conclusions

In conclusion, we have investigated the local through-film and lateral conductivity of large-grained (*ca.* 1 μm diameter) active layers that result in > 17% power conversion efficiency. While several studies have investigated the electrical properties of GBs at the top surface of MAPbI₃ films, this is the first study to examine how subsurface GB properties affect lateral movement of charges between grains. The data suggests that GBs exhibit a depth-dependent resistance ($R_{\text{GB}}(z)$), where all GBs are highly resistive at the top surface of the film, but lower resistance pathways across GBs exist below the surface. Furthermore, the electrical response of the lateral measurements indicates that the apparent grain size observed in the topography data corresponds to the true grain size.

While it has been implied in the literature that electrical conductivity along GBs plays a beneficial role for efficiently collecting photogenerated current, the results presented in this work clearly indicate that photocurrent collection along GBs is not a prerequisite for high-efficiency PSCs. Our results instead indicate that the electrical properties of GBs vary as a function of depth into the thickness of the MAPbI₃ layer, and from GB-to-GB. Assuming that the GB electrical properties (*e.g.* electrical resistance and band-bending) result in reduced recombination in these films, as suggested by several authors,^{14,15,23} the results presented herein indicate that improved control of the depth dependence of GB electrical properties, as well as the GB-to-GB electrical property homogeneity, may be crucial for further advances in the efficiency and performance of PSC devices.

Acknowledgements

Specific commercial equipment, instruments, and materials that are identified in this report are listed in order to adequately describe the experimental procedure and are not intended to imply endorsement or recommendation by the National Institute of Standards and Technology (NIST). Contribution of NIST, an agency of the U.S. government; not subject to copyright. Unless otherwise noted, experimental uncertainties are one standard deviation of the mean.

References

- 1 A. Kojima, K. Teshima, Y. Shirai and T. Miyasaka, *J. Am. Chem. Soc.*, 2009, **131**, 6050–6051.
- 2 H.-S. Kim, C.-R. Lee, J.-H. Im, K.-B. Lee, T. Moehl, A. Marchioro, S.-J. Moon, R. Humphry-Baker, J.-H. Yum, J. E. Moser, M. Grätzel and N.-G. Park, *Sci. Rep.*, 2012, **2**, 591.
- 3 M. Grätzel, *Nat. Mater.*, 2014, **13**, 838–842.
- 4 M. A. Green, A. Ho-Baillie and H. J. Snaith, *Nat. Photonics*, 2014, **8**, 506–514.
- 5 H. S. Jung and N.-G. Park, *Small*, 2015, **11**, 10–25.
- 6 Y. Zhao and K. Zhu, *J. Phys. Chem. Lett.*, 2014, **5**, 4175–4186.
- 7 T. Salim, S. Sun, Y. Abe, A. Krishna, A. C. Grimsdale and Y. M. Lam, *J. Mater. Chem. A*, 2015, **3**, 8943–8969.
- 8 W. Zhu, C. Bao, Y. Wang, F. Li, X. Zhou, J. Yang, B. Lv, X. Wang, T. Yu and Z. Zou, *Dalton Trans.*, 2016, **45**, 7856–7865.
- 9 http://www.nrel.gov/ncpv/images/efficiency_chart, 2016.
- 10 C. Li, Y. Wu, J. Poplawsky, T. J. Pennycook, N. Paudel, W. Yin, S. J. Haigh, M. P. Oxley, A. R. Lupini, M. Al-Jassim, S. J. Pennycook and Y. Yan, *Phys. Rev. Lett.*, 2014, **112**, 156103.
- 11 M. Gloeckler, J. R. Sites and W. K. Metzger, *J. Appl. Phys.*, 2005, **98**, 113704.
- 12 T. H. DiStefano and J. J. Cuomo, *Appl. Phys. Lett.*, 1977, **30**, 351.
- 13 D. W. de Quilettes, S. M. Vorpahl, S. D. Stranks, H. Nagaoka, G. E. Eperon, M. E. Ziffer, H. J. Snaith and D. S. Ginger, *Science*, 2015, **348**, 683–686.
- 14 J. S. Yun, A. Ho-Baillie, S. Huang, S. H. Woo, Y. Heo, J. Seidel, F. Huang, Y.-B. Cheng and M. A. Green, *J. Phys. Chem. Lett.*, 2015, **6**, 875–880.
- 15 Q. Chen, H. Zhou, T. Song, S. Luo, Z. Hong, H.-S. Duan, L. Dou, Y. Liu and Y. Yang, *Nano Lett.*, 2014, **14**, 4158–4163.
- 16 Y. Shao, Z. Xiao, C. Bi, Y. Yuan and J. Huang, *Nat. Commun.*, 2014, **5**, 5784.
- 17 Y. Shao, Y. Fang, T. Li, Q. Wang, Q. Dong, Y. Deng, Y. Yuan, H. Wei, M. Wang, A. Gruverman, J. Shield and J. Huang, *Energy Environ. Sci.*, 2016, **9**, 1752–1759.
- 18 C. G. Bischak, E. M. Sanehira, J. T. Precht, J. M. Luther and N. S. Ginsberg, *Nano Lett.*, 2015, **15**, 4799–4807.
- 19 M. Yang, Y. Zhou, Y. Zeng, C.-S. Jiang, N. P. Padture and K. Zhu, *Adv. Mater.*, 2015, **27**, 6363–6370.
- 20 W. Ke, C. Xiao, C. Wang, B. Saparov, H. Duan, D. Zhao, Z. Xiao, P. Schulz, S. P. Harvey, W. Liao, W. Meng, Y. Yu, A. J. Cimaroli, C. Jiang, K. Zhu, M. Al-Jassim, G. Fang, D. B. Mitzi and Y. Yan, *Adv. Mater.*, 2016, **28**, 5214–5221.
- 21 K. L. Johnson and L. M. Keer, *J. Tribol.*, 1986, **108**, 659.
- 22 A. Bietsch, M. A. Schneider, M. E. Welland and B. Michel, *J. Vac. Sci. Technol., B: Microelectron. Nanometer Struct.*, 2000, **18**, 1160.
- 23 J. Li, J.-Y. Ma, Q.-Q. Ge, J. Hu, D. Wang and L.-J. Wan, *ACS Appl. Mater. Interfaces*, 2015, **7**, 28518–28523.
- 24 J. A. Christians, P. A. Miranda Herrera and P. V. Kamat, *J. Am. Chem. Soc.*, 2015, **137**, 1530–1538.

- 25 A. M. A. Leguy, Y. Hu, M. Campoy-Quiles, M. I. Alonso, O. J. Weber, P. Azarhoosh, M. van Schilfgaarde, M. T. Weller, T. Bein, J. Nelson, P. Docampo and P. R. F. Barnes, *Chem. Mater.*, 2015, **27**, 3397–3407.
- 26 D. Li, S. A. Bretschneider, V. W. Bergmann, I. M. Hermes, J. Mars, A. Klasen, H. Lu, W. Tremel, M. Mezger, H.-J. Butt, S. A. L. Weber and R. Berger, *J. Phys. Chem. C*, 2016, **120**, 6363–6368.
- 27 M. Rezeq, K. Eledlebi, M. Ismail, R. K. Dey and B. Cui, *J. Appl. Phys.*, 2016, **120**, 044302.
- 28 O. G. Reid, M. Yang, N. Kopidakis, K. Zhu and G. Rumbles, *ACS Energy Lett.*, 2016, 561–565.
- 29 J. M. Frost, K. T. Butler, F. Brivio, C. H. Hendon, M. van Schilfgaarde and A. Walsh, *Nano Lett.*, 2014, **14**, 2584–2590.
- 30 G. Niu, W. Li, F. Meng, L. Wang, H. Dong and Y. Qiu, *J. Mater. Chem. A*, 2014, **2**, 705.